Amino Acid Residues in the Nicotinamide Binding Site Contribute to Catalysis by Horse Liver Alcohol Dehydrogenase[†,‡]

Jon K. Rubach and Bryce V. Plapp*

Department of Biochemistry, The University of Iowa, Iowa City, Iowa 52242

Received November 28, 2002; Revised Manuscript Received January 21, 2003

ABSTRACT: Amino acid residues Thr-178, Val-203, and Val-292, which interact with the nicotinamide ring of the coenzyme bound to alcohol dehydrogenase (ADH), may facilitate hydride transfer and hydrogen tunneling by orientation and dynamic effects. The T178S, T178V, V203A, V292A, V292S, and V292T substitutions significantly alter the steady state and transient kinetics of the enzyme. The V292A, V292S, and V292T enzymes have decreased affinity for coenzyme (NAD^+ by 30−50-fold and NADH by 35−75-fold) as compared to the wild-type enzyme. The substitutions in the nicotinamide binding site decrease the rate constant of hydride transfer for benzyl alcohol oxidation by 3-fold (for V292T ADH) to 16-fold (for V203A ADH). The modest effects suggest that catalysis does not depend critically on individual residues and that several residues in the nicotinamide binding site contribute to catalysis. The structures of the V292T ADH−NAD^+−pyrazole and wild-type ADH−NAD^+−4-iodopyrazole ternary complexes are very similar. Only subtle changes in the V292T enzyme cause the large changes in coenzyme binding and the small change in hydride transfer. In these complexes, one pyrazole nitrogen binds to the catalytic zinc, and the other nitrogen forms a partial covalent bond with C4 of the nicotinamide ring, which adopts a boat conformation that is postulated to be relevant for hydride transfer. The results provide an experimental basis for evaluating the contributions of dynamics to hydride transfer.

Experimental and computational studies suggest that dynamic motions facilitate hydride transfer catalyzed by alcohol dehydrogenase (*1*−*5*). Hydride transfer occurs with hydrogen tunneling (*6*−*9*), which occurs as the distance between hydride donor and acceptor atoms, the α-carbon of the alcohol and the C4 of the nicotinamide ring of NAD^+, becomes about 2.7 Å (*4*). The distance between the carbon atoms in the pentafluorobenzyl alcohol ternary complex, which is thought to mimic the Michaelis complex, is 3.4 Å (*10*). Therefore, the substrates must move closer together for tunneling to occur. Some of the decrease in distance may be due to the normal fluctuations of the substrates. The nicotinamide ring could also adopt a boat conformation, which should facilitate the overlap of the molecular orbitals at the transition state and decrease the energy barrier between the ground state and the transition state (*11*−*13*).

The amino acid residues in the nicotinamide binding site of alcohol dehydrogenase (ADH),[1] Val-292, Thr-178, and Val-203, make close contacts with the face of the nicotinamide ring that is not involved in hydride transfer (Figure 1). If the motions of the protein are involved in facilitating the reaction, the residues in the nicotinamide binding site may distort the nicotinamide ring. Amino acid substitutions at Val-203 have been shown to decrease the extent of hydrogen tunneling in the catalyzed reaction (*8*), which suggests that the substitution affects the hydride transfer step. However, the effects of the substitution on the rate constants of hydride transfer have not been determined. Substituting the amino acids in the nicotinamide binding site and determining the effects on the structure and mechanism can define the contributions of these residues to catalysis.

EXPERIMENTAL PROCEDURES

Materials. Wild-type crystalline horse liver alcohol dehydrogenase (EE isoenzyme), $LiNAD^+$, and Na_2NADH were purchased from Roche Molecular Biochemicals. Pyrazole was purchased from Aldrich and 4-iodopyrazole from Sigma. Benzyl alcohol-α,α-d_2 (98.6% D) was from MSD Isotopes. (4*R*)-[4-^{2}H]NADD was prepared from NAD^+ and ethanol-d_6 (Aldrich, 99+% D) with yeast alcohol dehydrogenase (*14*) and purified on a DEAE-Sepharose column developed with a linear gradient of 10−250 mM sodium phosphate buffer, pH 8. The benzyl alcohol and benzaldehyde purchased from Fisher Scientific were redistilled before use.

Preparation of the Enzymes. The ADH enzymes with substitutions at Val-292 and Thr-178 were created by partially random mutagenesis, using the plasmid pBPP/*Eq*ADH (*15*) and the Stratagene Quick Change method. The plasmid for the V203A-substituted enzyme was obtained from Dr. Judith P. Klinman (*8*). The degenerate oligodeoxy-

[†] This work was supported NIH Grants T32 GM08365 and AA00279 and NSF Grant MCB 95-06831.

[‡] The X-ray coordinates and structure factors have been deposited in the RCSB Protein Data Bank with the entry names 1N92 for the wild-type enzyme complexed with NAD^+ and 4-iodopyrazole and 1N8K for the V292T enzyme complexed with NAD^+ and pyrazole.

* Corresponding author. Phone: 319-335-7909. Fax: 319-335-9570. E-mail: bv-plapp@uiowa.edu.

[1] Abbreviations: ADH, alcohol dehydrogenase; PFB, 2,3,4,5,6-pentafluorobenzyl alcohol; PYZ, pyrazole; V292S, substitution of Val-292 with Ser; V292A, substitution of Val-292 with Ala; V292T, substitution of Val-292 with Thr; T178S, substitution of Thr-178 with Ser; T178V, substitution of Thr-178 with Val; V203A, substitution of Val-203 with Ala; rmsd, root-mean-square deviation.

10.1021/bi0272656 CCC: $25.00
Published on Web 02/20/2003

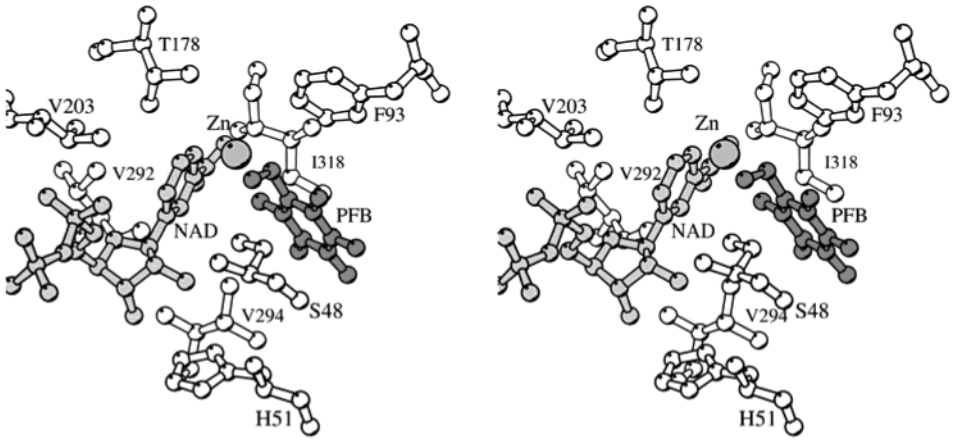

FIGURE 1: Stereo representation of the active site of horse liver alcohol dehydrogenase. Residues Val-292, Val-203, and Thr-178 are in the nicotinamide binding pocket. Pentafluorobenzyl alcohol, the nicotinamide ribose of NAD^+, and the catalytic zinc are shown in gray. The coordinates are from PBD entry 1HLD (*10*).

ribonucleotide mutamers were synthesized by Life Technologies, Inc. The mutamers used for the Thr-178 substitutions had the following sequences, where the underlines mark the sites of mutation: GGC TGT GGA TTT TCT (T/G)(C/T)T GGT TAT GGG TCT GCA GTC and GAC TGC AGA CCC ATA ACC A(A/G)(A/C) AGA AAA TCC ACA GCC. The mutamers used for the Val-292 substitutions had the following sequences: GCA TAT GGT GTG AGC GTA ATT (G/A)(T/C/G)C GGA GTA CCT CCT GAT TCC and CGT ATA CCA CAC TCG CAT TAA (C/T)(A/G/C)G CCT CAT GGA GGA CTA AGG. After transformation in XL1-Blue cells and selection for ampicillin- and tetracycline-resistant colonies, plasmids were isolated, and mutations were identified by the loss of restriction endonuclease sites. The Thr-178 mutations caused the loss of a *Bsr*I restriction site (ACTGGN), and the Val-292 mutations caused the loss of an *Hga*I restriction site (CGCAG). The mutations were confirmed by complete sequencing of the ADH cDNAs by The University of Iowa DNA Facility. The enzymes were expressed and purified according to the published procedure (*15*) and were judged to be more than 95% pure as determined by polyacrylamide gel electrophoresis in the presence of sodium dodecyl sulfate.

Kinetic Studies. The studies used 33 mM sodium phosphate and 0.25 mM EDTA buffer, pH 8, at 25 °C. The concentration of enzyme active sites was determined by titration with NAD^+ in the presence of pyrazole (*16*). The standard assay (*17*) was used to determine the specific activities of the substituted enzymes. Coenzyme concentrations were determined by absorbance at 260 or 340 nm. Enzyme activities were determined on a Cary 118C spectrophotometer or an SLM 4800C fluorometer ($\lambda_{ex} = 340$ nm, $\lambda_{em} = 460$ nm), with computer fitting of the progress curves to obtain the initial velocities. The initial velocity data for the oxidation of benzyl alcohol and reduction of benzaldehyde with systematically varied concentrations of coenzyme and substrate were fitted to the equation for a sequential bi mechanism. Dissociation constants for coenzymes and inhibitors were determined by inhibition studies. The isotope effects on steady-state kinetic parameters were obtained by comparing the rate constants for the protio and deuterio substrates. The steady-state kinetic data were fitted using Cleland's programs (*18*).

A BioLogic SFM3 stopped-flow instrument (dead time of 2.4 ms) was used to study the transient kinetics. Binding of NAD^+ was monitored by the increase in absorbance at 294 nm due to the formation of the enzyme−NAD^+−pyrazole complex (*19*), and the binding of NADH was studied by the quenching of protein fluorescence ($\lambda_{ex} = 294$ nm, $\lambda_{em} = 310-384$ nm) in the presence of *N*-cyclohexylformamide, an aldehyde analogue (*20*, *21*). The rates of coenzyme binding were measured for varied concentrations of NAD^+ and pyrazole or NADH and *N*-cyclohexylformamide. The progress curves were analyzed by the BioKine software and fitted a first-order process. The bimolecular rate constants were calculated from the first-order dependence on coenzyme concentration. NADH binding to the T178S and V203A enzymes was studied without using *N*-cyclohexylformamide, and the microscopic rate constants for the binding reactions were determined by progress curve analysis through the use of the kinetic simulation program, KINSIM, and the automatic fitting routine, FITSIM (*22*). The transient oxidation reactions were followed by the change in absorbance at 328 nm upon the mixing of 10 μN enzyme with NAD^+ and varied concentrations of benzyl alcohol or benzyl alcohol-α,α-d_2. The maximum rate constant was calculated by fitting the data to the equation for a hyperbola. An extinction coefficient of 5500 M^{-1} cm^{-1} at 328 nm was used for the difference in absorption of NADH and NAD^+ bound to the enzyme and its complexes (*23*).

X-ray Crystallography. The crystals of wild-type ADH complexed with NAD^+ and 4-iodopyrazole were prepared as described by the general procedure used previously (*10*). Horse liver enzyme from Boehringer Mannheim Corp. (Roche) was recrystallized from 10% ethanol, and the crystals were redissolved and dialyzed against 50 mM ammonium *N*-[tris(hydroxymethyl)methyl]-2-aminoethanesulfonate buffer and 0.25 mM EDTA, pH 6.7 (measured at 25 °C). About 1 mL of 10 mg/mL enzyme was dialyzed at 4 °C against 10 mL of the same buffer with 1 mM NAD^+ and 1 mM 4-iodopyrazole ($K_i = 0.02$ μM; *24*) as the concentration of 2-methyl-2,4-pentanediol was raised over some days to 16% when crystals formed. The concentration of the diol was finally raised to 25%. The spectrum of the outer dialyzate showed that NAD^+, and no NADH, was present.

Table 1: Steady-State Kinetic Constants for the Activity on Benzyl Alcohol and Benzaldehyde of Alcohol Dehydrogenases with Substitutions in the Nicotinamide Binding Site[a]

kinetic constant	rADH[b]	T178S	T178V	V203A	V292A	V292S[c]	V292T
K_a (μM)	3.7	1.6	30	6.8	79	140	92
K_b (μM)	23	12	29	94	140	220	270
K_p (μM)	30	11	730	65	290	440	480
K_q (μM)	1.7	0.95	2.9	10	35	80	40
K_{ia} (μM)	31	14	260	29	1100	1600	930
K_{iq} (μM)	0.4	0.5[d]	1.8	2.1	14	30	19
V_1 (s^{-1})	2.2	1.0	3.9	2.2	4.9	6.3	9.3
V_2 (s^{-1})	22	8.0	65	30	91	160	190
V_1/K_b (mM^{-1} s^{-1})	96	81	130	23	35	28	35
V_2/K_p (mM^{-1} s^{-1})	700	720	90	460	320	360	400
K_{eq} (pM)[e]	44	43	100	37	14	32	18
turnover no. (s^{-1})[f]	1.1	0.54	2.3	4.6	24	34	49
$K_{i,AMP}$ (μM)	44[g]				80	86	40
$K_{i,pentafluorobenzyl\ alcohol}$ (μM)	3.0[h]		7.8	1.9	9.0	2.0	5.5
$K_{i,cyclohexylformamide}$ (μM)	9.0[i]				19	11	23

[a] Kinetic constants were determined at 25 °C in 33 mM sodium phosphate and 0.25 mM EDTA buffer, pH 8.0. K_a, K_b, K_p, and K_q are the Michaelis constants for NAD^+, benzyl alcohol, benzaldehyde, and NADH, respectively. K_{ia} and K_{iq} are the dissociation constants for NAD^+ and NADH, respectively. V_1 is the turnover number for benzyl alcohol oxidation, and V_2 is the turnover number for benzaldehyde reduction. The standard errors of the fitted values are <25%, which indicates that the values are well determined (*18*). Replicate experiments usually give values within 2-fold of those reported. [b] rADH is recombinant wild-type alcohol dehydrogenase; from ref *5*. [c] From ref *5*. [d] Calculated from the rate constants for NADH binding (Table 3) because the initial velocity pattern had parallel lines. [e] K_{eq} is equilibrium constant calculated from the Haldane relationship, $V_1K_pK_{iq}[H^+]/V_2K_bK_{ia}$. Values for the equilibrium constant have been estimated to be 35−70 pM (*48*−*50*). [f] Turnover number determined in a standard enzyme assay at 25 °C (*17*) based on titration of active sites. [g] From ref *51*. [h] From ref *52*. [i] From ref *20*.

The crystals of the V292T ADH−NAD^+−pyrazole ternary complex were produced by dialysis of 15 mg/mL enzyme against 17% 2-methyl-2,4-pentanediol in 50 mM ammonium *N*-[tris(hydroxymethyl)methyl]-2-aminoethanesulfonate buffer and 0.25 mM EDTA, pH 6.7 (measured at 25 °C), with 10.6 mM NAD^+ and 5.5 mM pyrazole. The final concentration of 2-methyl-2,4-pentanediol was raised to 24%.

The crystals for both complexes were flash cooled in liquid N_2, and the X-ray data were collected at 100 K. The data for the wild-type ADH−NAD^+−4-iodopyrazole complex were collected on an R-Axis IV++ area detector with a rotating anode generator and processed with d*TREK (*56*). The data for the V292T ADH−NAD^+−pyrazole complex were collected at the 19-ID IMCA-CAT beam line at the Advanced Photon Source and processed using HKL2000 (*25*). Both structures were solved by molecular replacement using AMORE (*26*) and the coordinates for the refined wild-type ADH−NAD^+−2,3,4,5,6-pentafluorobenzyl alcohol complex (1HLD) as a model (*10*). The AMORE program was configured with the catalytic domains (residues 1−175, 319−374) and coenzyme binding domains (residues 176−318) treated independently of each other. The structures were refined by cycles of restrained refinement with REFMAC (*27*) and model building with the program O (*28*). Model bias was avoided during the initial refinement by making residue 292 an alanine and by not adding NAD^+ and pyrazole or 4-iodopyrazole to the model. The V292T substitution was made, and the NAD^+ and pyrazole were added only after the electron density maps clearly showed the positions for the ligands. Initially, the nicotinamide ring in the NAD^+ molecule dictionary was set to be planar for both models. However, the $2F_o - F_c$ and $F_o - F_c$ electron density maps clearly showed that the nicotinamide rings were not planar in these structures, and therefore the monomer dictionary used by REFMAC was modified to remove the restraints on planarity and torsion angles for the nicotinamide ring. The modified coenzyme is named NAJ in the coordinate files in order to distinguish it from the NAD listed in other structures.

RESULTS

Steady-State Kinetics of Substituted Enzymes. The initial velocity patterns for the forward reaction (NAD^+ and benzyl alcohol), the reverse reaction (NADH and benzaldehyde), and the product and dead-end inhibition studies with the substituted enzymes are all consistent with an ordered bi-bi sequential kinetic mechanism (data not shown). The steady-state kinetic constants for the substituted enzymes are summarized in Table 1.

The kinetic constants of the T178S enzyme do not differ significantly from those of the wild-type enzyme. The T178V substitution increases V_1 and V_2 (the turnover numbers for alcohol oxidation and aldehyde reduction, respectively) by 2−3-fold but decreases V_2/K_p (the catalytic efficiency for benzaldehyde) by 8-fold (Table 1).

The V203A enzyme also has steady-state kinetics similar to those of the wild-type enzyme, except that K_{iq} (dissociation constant for NADH) is increased 5-fold (Table 1). The kinetic constants determined for the V203A enzyme differ from those previously reported ($V_1 = 0.2$ s^{-1}, $K_b = 1.0$ mM) where 300 mM potassium phosphate buffer, pH 7.0, containing 300 mM semicarbazide hydrochloride was used (*8*). We obtain kinetic constants similar to the published values when our V203A enzyme preparations are assayed in the 300 mM buffer and semicarbazide conditions.

The substitutions at Val-292 substantially decrease the affinity for the coenzymes, as determined by inhibition studies (K_{ia}, NAD^+, by 30−50-fold; K_{iq}, NADH, by 35−75-fold; Table 1). These enzymes bind AMP with affinities similar to that of the wild-type enzyme, which suggests that the binding of the AMP moiety of the coenzymes does not account for the changes in coenzyme affinity. The substitutions at Val-292 increase V_1 by 2−4-fold and V_2 by 4−9-fold. However, the substitutions have modest effects on V_2/K_p and V_1/K_b, which decrease 2- and 3-fold, respectively. Despite the large effects on coenzyme binding, the kinetic mechanisms appear to be ordered bi-bi, as for the wild-type enzyme. Pentafluorobenzyl alcohol produces competitive

Table 2: Substrate Isotope Effects on Benzyl Alcohol Oxidation and Benzaldehyde Reduction Catalyzed by Alcohol Dehydrogenases

isotope effect[a]	wild type[b]	T178S[c]	T178V[d]	V203A[e]	V292A[f]	V292S[g]	V292T[h]
$^{D}V_1$	1.4 ± 0.1	2.3 ± 0.2	1.6 ± 0.3	3.4 ± 0.2	4.0 ± 0.1	4.3 ± 0.7	3.6 ± 0.2
$^{D}V_1/K_b$	1.6 ± 0.5	4.4 ± 0.4	2.6 ± 0.6	4.1 ± 0.6	3.8 ± 0.3	3 ± 1	4.1 ± 0.6
$^{D}V_2$	1.1 ± 0.1			1.1 ± 0.1	1.2 ± 0.1	1.3 ± 0.1	1.7 ± 0.1
$^{D}V_2/K_p$	1.6 ± 0.5			3.1 ± 0.5	2.8 ± 0.2	3.1 ± 0.2	3.4 ± 0.3

[a] The superscript D represents the ratio of kinetic constants with protio and deuterio substrates. [b] From ref *53*. [c] Substrate concentrations were 2 mM NAD^+ and 8−100 μM benzyl alcohol or 2 mM NAD^+ and 12−150 μM benzyl alcohol-α,α-d_2. [d] Substrate concentrations were 15−130 μM NAD^+ and 10−100 μM benzyl alcohol or 14−120 μM NAD^+ and 30−260 μM benzyl alcohol-α,α-d_2. [e] Substrate concentrations were 10−100 μM NAD^+ and 70−610 μM benzyl alcohol or 10−100 μM NAD^+ and 130−1200 μM benzyl alcohol-α,α-d_2, 1.7−16 μM NADH and 17−150 μM benzaldehyde or 1.7−15 μM NADD and 30−300 μM benzaldehyde. [f] Substrate concentrations were 90−800 μM NAD^+ and 100−910 μM benzyl alcohol or 90−820 μM NAD^+ and 155−1400 μM benzyl alcohol-α,α-d_2, 21−185 μM NADH and 190−1700 μM benzaldehyde or 19−175 μM NADD and 550−5000 μM benzaldehyde. [g] Substrate concentrations were 70−620 μM NAD^+ and 640−5800 μM benzyl alcohol or 80−720 μM NAD^+ and 150−1400 μM benzyl alcohol-α,α-d_2, 20−200 μM NADH and 250−2200 μM benzaldehyde or 25−230 μM NADD and 400−3500 μM benzaldehyde. [h] Substrate concentrations were 40−380 μM NAD^+ and 160−1500 μM benzyl alcohol or 40−380 μM NAD^+ and 240−2200 μM benzyl alcohol-α,α-d_2, 20−190 μM NADH and 360−3200 μM benzaldehyde or 20−150 μM NADD and 440−4000 μM benzaldehyde.

Table 3: Rate Constants for Transient Reactions of Alcohol Dehydrogenases

rate constant	wild type[a]	T178S	T178V	V203A	V292A	V292S	V292T
k_{on,NAD^+} ($\mu M^{-1}\,s^{-1}$)[b]	1.2	1.4 ± 0.2			0.15 ± 0.01	0.11 ± 0.03	0.25 ± 0.06
k_{off,NAD^+} (s^{-1})	36	20[c]			170[c]	180[c]	230[c]
$k_{on,NADH}$ ($\mu M^{-1}\,s^{-1}$)[b]	11	12 ± 0.1		3.7 ± 0.1	9 ± 3	7 ± 2	13 ± 2.3
$k_{off,NADH}$ (s^{-1})	5.5	6.2 ± 0.1		20 ± 1	130[c]	210[c]	250[c]
$k_{max,oxidation}$(s^{-1})[d]	24 ± 3	2.6 ± 0.1[e]	29 ± 1[f]	1.5 ± 0.2[g]	4.9 ± 0.7[h]	6.3 ± 0.6[i]	9 ± 1[j]
$^{D}k_{max,oxidation}$[k]	3.6 ± 0.5	3.1 ± 0.2	3.8 ± 0.4	3.8 ± 0.4	3.5 ± 0.3	4.3 ± 0.3	3.6 ± 0.2

[a] From ref *29*. [b] 1 $\mu M^{-1}\,s^{-1} = 1 \times 10^6\ M^{-1}\,s^{-1}$. [c] Calculated from $k_{off} = k_{on}(K_{ia})$ or $k_{on}(K_{iq})$. K_{ia} and K_{iq} are from Table 1. [d] Maximum rate constants for the transient oxidation of benzyl alcohol. [e] Substrate concentrations were 2 mM NAD^+ and 0.16−3 mM benzyl alcohol. [f] Substrate concentrations were 5 mM NAD^+ and 0.25−1.5 mM benzyl alcohol. [g] Substrate concentrations were 10 mM NAD^+ and 0.46−10 mM benzyl alcohol. [h] Substrate concentrations were 10 mM NAD^+ and 50−1000 μM benzyl alcohol. [i] Substrate concentrations were 5 mM NAD^+ and 0.26−5.0 mM benzyl alcohol. [j] The k_{max} is the V_1 from the steady-state data. [k] The superscript D represents the ratio of kinetic constants with protio and deuterio substrates.

inhibition against benzyl alcohol as the varied substrate and uncompetitive inhibition against NAD^+ as the varied substrate. Likewise, *N*-cyclohexylformamide produces competitive inhibition against benzaldehyde as the varied substrate and uncompetitive inhibition against NADH as the varied substrate. The dissociation constants for these substrate analogues are similar for the wild-type and mutated enzymes, suggesting that the substrate binding sites are not affected by the mutations.

All of the substituted enzymes have increased substrate kinetic isotope effects for benzyl alcohol oxidation (Table 2). The enzymes with substitutions at Val-292 and the V203A enzyme also have increased kinetic isotope effects for benzaldehyde reduction. The increased isotope effects for the steady-state reactions suggest that hydride transfer has become more rate limiting for the substituted enzymes. The amino acid substitutions in the nicotinamide binding site do not drastically alter the catalytic efficiencies or kinetic mechanisms of the enzymes but have unmasked the hydride transfer steps. Release of coenzymes in each direction is rate limiting for turnover by the wild-type enzyme, but hydride transfer is more rate limiting for the substituted enzymes.

Kinetics of Transient Reactions. Transient kinetics were used to determine how the rate constants for the binding of the coenzymes were affected in the substituted alcohol dehydrogenases (Table 3). The V292A, V292S, and V292T substitutions decrease the bimolecular rate constant for binding of NAD^+ by 5−10-fold as compared to the wild-type enzyme, but they do not affect the rate constant for the binding of NADH. The rate constants calculated for dissociation of coenzymes (k_{off,NAD^+} and $k_{off,NADH}$) from the V292A, V292S, and V292T enzymes increase as compared to those for wild-type enzyme (Table 3), accounting for increased turnover numbers (Table 1).

The transient oxidation of benzyl alcohol was studied to determine the effects of the substitutions on the rate constant for hydride transfer. The substitutions decrease the rate constants for the transient oxidation of benzyl alcohol ($k_{max,oxidation}$) by up to 16-fold (Table 3). The transient reaction with the wild-type enzyme shows an initial "burst" of NADH formation that is controlled by hydride transfer, followed by a steady-state phase controlled by release of NADH from the enzyme−NADH complex (*29*, *30*). The reactions with the T178S and T178V enzymes show burst phases for the transient oxidation of benzyl alcohol, which suggests that coenzyme release is rate limiting for the overall oxidation. In contrast, the reactions for the oxidation of benzyl alcohol by the V203A, V292A, V292S, and V292T enzymes have no observable burst phase, and together with the observation of significant isotope effects on V_1 (Table 2), the results suggest that hydride transfer is significantly rate limiting for the turnover of benzyl alcohol catalyzed by these enzymes.

The rate constants for the transient reduction of benzaldehyde by wild-type and substituted enzymes were too fast to determine with the BioLogic instrument. For the wild-type enzyme, the rate constant is 320 s^{-1} (*29*). The small isotope effects on V_2 and the similar values of the calculated rate constants for NAD^+ release (k_{off,NAD^+}) and the turnover numbers (V_2) suggest that NAD^+ release is the rate-limiting step for the overall reduction of benzaldehyde. Therefore, the rate constants for hydride transfer to benzaldehyde are at least as large as the turnover numbers and do not seem to

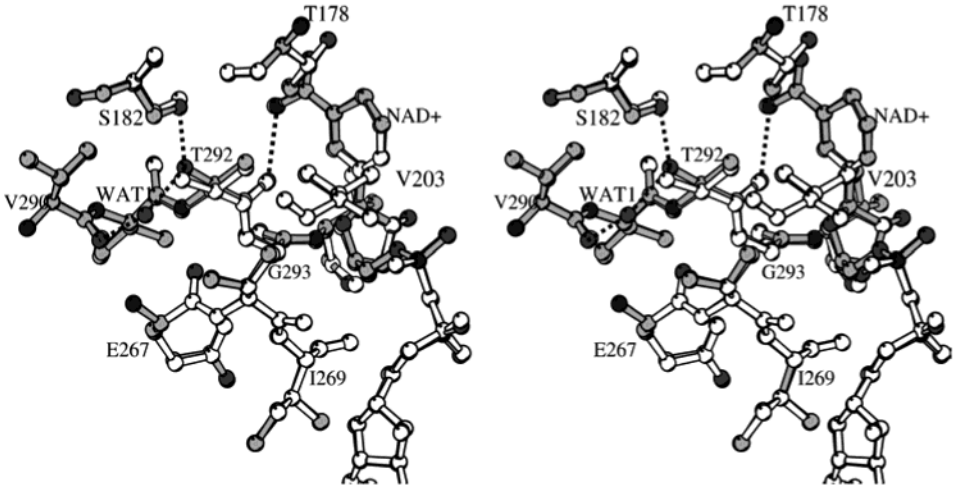

FIGURE 2: Superposition of the V292T ADH−NAD−pyrazole (gray) and the wild-type ADH−NAD−4-iodopyrazole (white) complexes. Amino acid residues adjacent to the site of the V292T substitution are shown. The OG1 of Thr-292 forms a hydrogen bond with the OG of Ser-182 and a new water molecule (WAT1), which hydrogen bonds to the carbonyl oxygen of Val-290. The steric contacts of the different enzymes with the nicotinamide ring are essentially the same.

be affected as much by the substitutions as are the constants for benzyl alcohol oxidation.

X-ray Crystallography. The structure of the V292T ADH complexed with NAD^+ and pyrazole was determined so that the structural basis for the changes in the hydride transfer and coenzyme dissociation rate constants could be evaluated. For comparison, we also determined the structure of the wild-type ADH−NAD^+−iodopyrazole complex at high resolution (to 1.5 Å). Complexes of wild-type horse ADH with NAD^+−pyrazole and NAD^+−iodopyrazole were previously solved at 2.9 Å resolution (*31*), and structures for the human class 1B (β isoenzyme) complexed with 4-iodopyrazole have been solved to 2.4 or 2.2 Å (*32*, *33*). The V292T ADH−NAD^+−pyrazole and the wild-type ADH−NAD^+−iodopyrazole complexes both crystallized in a triclinic space group that contains one dimeric molecule in the asymmetric unit. The X-ray data and refinement statistics for the structures are given in Table 4. The crystal of the V292T ADH−NAD^+−pyrazole complex diffracted to 1.13 Å with the data being 46% complete in the highest resolution shell and 68% complete for the 1.27−1.22 Å resolution shell. All of the data were used during refinement.

The wild-type ADH−NAD^+−iodopyrazole and V292T ADH−NAD^+−pyrazole complexes have the "closed" conformation and are isomorphous with the complexes of wild-type ADH with NAD^+ and pyrazole or 4-iodopyrazole determined previously (*31*). The protein structures of the V292T ADH−pyrazole and wild-type ADH−iodopyrazole complexes are almost identical. Thr-292 adopts the same rotamer conformation as Val-292, and the carbonyl oxygen of these residues forms a hydrogen bond with the nitrogen in the carboxamido group of the nicotinamide ring (Figure 2). The hydroxyl group of Thr-292 forms hydrogen bonds with the hydroxyl group of Ser-182 and with a new water molecule, which is also hydrogen bonded to the carbonyl oxygen of Val-290. A similar water molecule is hydrogen bonded to the OG of Ser-292 and the carbonyl oxygen of Val-290 in the structure of the V292S enzyme (*5*). The V292T enzyme has a hydrogen bond between Thr-292 and Ser-182 at 2.94 Å as compared to the wild-type enzyme that has a van der Waals contact of 3.44 Å between CG2 of Val-292 and OG of Ser-182.

Table 4: X-ray Data and Refinement Statistics for Wild-Type and V292T Horse Liver Alcohol Dehydrogenases

enzyme	wild type	V292T
complex with NAD^+	4-iodopyrazole	pyrazole
PDB entry	1N92	1N8K
space group	P_1	P_1
molecules per unit cell	1	1
cell dimensions, Å	51.0, 92.5, 44.2	51.4, 92.7, 44.3
cell angles, deg	102.9, 109.8, 91.7	103.0, 109.9, 91.9
resolution range, Å	20.0−1.47	20−1.13
measured reflections: unique, total	109109, 227408	218390, 613593
completeness, % (outer shell)	88.8 (69)	81.6 (46.2)
R_{sym}, % (outer shell)[a]	5.4 (12.7)	5.8 (16.7)
mean $\langle I\rangle/\sigma\langle I\rangle$ (outer shell)	5.9 (4.1)	32 (6.4)
R_{value}, R_{free}, test %[b]	15.1, 18.3, 2.5	14.5, 16.7, 3.5
rsmd for bond distances, Å[c]	0.016	0.015
rmsd for bond angles, deg[c]	1.63	1.70
estd errors in coordinates, Å	0.042	0.023
no. of water molecules	581	707

[a] $R_{sym} = (\sum|F - \langle I\rangle|)/\sum\langle I\rangle$, where I is the integrated intensity of a given reflection. [b] $R_{value} = (\sum|F_o - kF_c|/\sum|F_o|$, where k is a scale factor. R_{free} (*54*) was calculated with the indicated percentage of reflections not used in the refinement. [c] Deviations from ideal geometry.

In both complexes, the NAD^+ and pyrazole molecules are bound in the same positions as seen previously (*31*−*33*), but the higher resolution yields more details on the bond distances and angles of the ligands. In both structures, N1 of the pyrazole ring is ligated to the active site zinc atom, and N2 of pyrazole forms a partial covalent bond with C4 of the nicotinamide in the NAD^+ with bond lengths of about 1.7 Å (Figure 3, Table 5). When the structures are refined using a model for the NAD^+−pyrazole complex that has the covalent bond between C4 and N2 fixed at 1.5 Å, the $F_o - F_c$ electron density maps clearly show difference densities that indicate that the C4−N2 bond distance must be longer than 1.5 Å.

NMR studies using ^{15}N-labeled pyrazole for the wild-type ADH−NAD^+−pyrazole complex also suggest that N2 of pyrazole forms a bond with the nicotinamide ring of NAD^+ (*34*). The partial covalent bond seen in these structures explains the shift in the UV absorption spectrum from 260 to 290 nm upon formation of the ADH−NAD^+−pyrazole

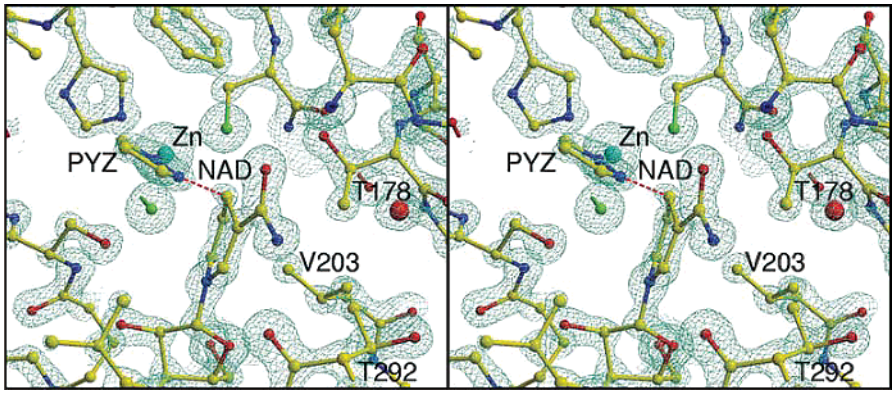

FIGURE 3: Puckered conformation of the nicotinamide ring of NAD in the V292T ADH−NAD−pyrazole ternary complex. The nicotinamide ring of NAD^+ forms a partial covalent bond, with the N2 in pyrazole (PYZ), with a distance of 1.7 Å (red dashed line). The $2F_o - F_c$ electron density map is shown contoured at 2.7σ.

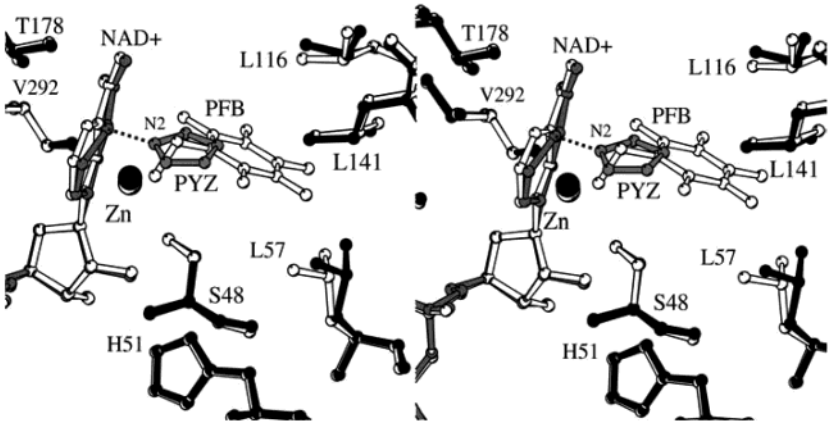

FIGURE 4: Effect of puckering on the distance between the reacting carbons. The active sites of the V292T ADH−NAD−pyrazole ternary complex (black and gray) and the wild-type ADH−NAD^+−2,3,4,5,6-pentafluorobenzyl alcohol ternary complex (white) determined to 1.1 Å (unpublished results) were superimposed. The overlay shows that the puckering of the nicotinamide ring could decrease the distance between the C4 of the nicotinamide ring and the α-carbon of the alcohol by about 0.7 Å.

complex (*16*, *31*). The spectrum of NADH bound to the enzyme has an absorption maximum at 325 nm (*16*). Thus, the absorption of the NAD^+−pyrazole complex at 290 nm is further evidence that the pyrazole has not formed a normal covalent bond with the NAD^+ in the ternary complex.

The nicotinamide ring in the NAD^+−pyrazole complexes adopts a boat conformation where the nicotinamide N1 and C4 atoms are not in the same plane as atoms C2, C3, C5, and C6 (Figure 3). The relevant angles and bond distances for the nicotinamide ring in the NAD^+−pyrazole complex are given in Table 5. Superimposing the coenzyme binding domains of the structures of the NAD^+−pyrazole complex and wild-type ADH complexed with NAD^+ and 2,3,4,5,6-pentafluorobenzyl alcohol (determined to 1.1 Å; unpublished results) shows that the puckering of the nicotinamide ring allows Thr-178 to move about 0.2 Å toward the nicotinamide ring (Figure 4). This small movement appears to be significant and shows that the protein can adopt conformations in which the residues could transiently strain the nicotinamide ring.

The V292S and V292T enzymes have similar kinetic constants and affinities for coenzyme (Table 1). However, the V292S enzyme crystallizes in the open form in the presence of NAD^+ and pentafluorobenzyl alcohol (*5*), whereas the V292T enzyme crystallizes in the closed form in the presence of NAD^+ and pyrazole. That V292T ADH crystallizes in a closed conformation may be due to the stabilization of the ternary complex by the formation of the NAD^+−pyrazole adduct. We concluded previously that the

Table 5: Geometry for the Nicotinamide Rings in the NAD^+−Pyrazole Complexes with V292T and Wild-Type Alcohol Dehydrogenases

	enzyme, ligand				
	V292T, pyrazole		wild type, 4-iodopyrazole		
	subunit A	subunit B	subunit A	subunit B	NAD^+ [a]
bond lengths (Å)					
N1−C2	1.36	1.35	1.36	1.38	1.346
C2−C3	1.35	1.37	1.43	1.45	1.391
C3−C4	1.53	1.52	1.52	1.53	1.398
C4−C5	1.47	1.45	1.52	1.49	1.384
C5−C6	1.31	1.35	1.32	1.33	1.379
C6−N1	1.37	1.41	1.36	1.48	1.347
C4−N2 (pyrazole)	1.70	1.73	1.76	1.75	
Zn−N1 (pyrazole)	2.14	2.15	2.22	2.20	
puckering geometry [b]					
αN1 (deg)	14.0	8.9	16.3	17.4	
αC4 (deg)	22.0	25.8	18.0	20.0	
twist (Å)	0.92	3.4	3.5	1.2	

[a] For the structure of the zwitterion determined by neutron diffraction at 0.65 Å (*55*). [b] αN1 describes the angle between the planes defined by atoms C2−N1−C6 and C2−C3−C6, αC4 is the angle between planes defined by atoms C3−C4−C5 and C2−C3−C6, and twist is the distortion of the boat as calculated by the distance in angstroms between C5 and the plane defined by atoms C2−C3−C6 (*39*).

V292S enzyme also adopts a closed conformation during catalysis (*5*).

DISCUSSION

Amino acid residues in the nicotinamide binding site are involved in the binding and preorganization of the nicotinamide ring for catalysis, but the quantitative contributions to catalysis need to be established. Decreasing the steric interactions of the protein with the nicotinamide ring should give the nicotinamide more room in which to move and may allow conformations that are not productive for hydride transfer. On the basis of the reported 40-fold decrease of $k_{cat}/K_{m,benzyl\ alcohol}$ with the V203A substituted enzyme (*8*), we expected that the substitutions would have large effects on the rate constants for hydride transfer. We further expected that the rate constants might correlate with the changes in the size of the side chain of the substituted residue. The kinetic studies on the alcohol dehydrogenases with substitutions in the nicotinamide binding pocket show that the substitutions have significant, but modest, effects on the catalytic efficiencies of the enzymes for the oxidation and reduction reactions (V_1/K_b, V_2/K_p; Table 1) and on the rate constants for hydride transfer for benzyl alcohol oxidation and for coenzyme binding (Table 3).

Effects of the Substitutions on Coenzyme Binding. Substitutions of Val-292 decreased affinities for NAD^+ and NADH (Table 1); decreases in k_{on,NAD^+} and increases in k_{off,NAD^+} and $k_{off,NADH}$ for the substituted enzymes can account for these effects (Table 3). As described previously for the V292S enzyme (*5*), the substitutions at position 292 probably decrease affinity for coenzyme by perturbing the equilibrium of the conformational change of the enzyme−coenzyme complex. When horse liver ADH binds coenzyme, a rotation of about 10° brings the catalytic domain closer to the coenzyme binding domain to create the closed form of the enzyme (*35*−*37*). For the wild-type enzyme, a limiting rate constant of 540 s^{-1} for binding of NAD^+ at saturating concentrations was observed, and rate constants for an isomerization, which is probably related to the conformational change, could be determined from analysis of the transient data (*19*). The rate constants for the binding of NAD^+ with the T178S, V292S, V292T, and V292A enzymes depended directly on NAD^+ concentration (up to 200 s^{-1}), and no limiting rate was observed with the stopped-flow instrument used in the present studies. Thus, a unique set of rate constants for the isomerization could not be determined. Nevertheless, the decreased affinities and rate constants for binding of NAD^+ and the increased turnover for benzaldehyde reduction (V_2) indicate that the substitutions at position 292 must increase the rate constant for the isomerization of the enzyme−NAD^+ complex from the closed to the "open" conformation. As discussed previously for the V292S enzyme, a 4-fold increase in the rate constant could account for the results (*5*). Similar analysis indicates that the substitutions of Val-292 could shift the equilibrium constant for "closing" from 10 to values in the range from 1 to 3.

The three-dimensional structure for the binary complex of the V292S enzyme with NAD is in the open conformation, whereas the structure for the ternary complex of the V292T enzyme is closed. Examination of the structures does not provide a simple explanation for the effects on coenzyme binding and the conformational equilibrium, which could arise because of effects in either conformational state. Nevertheless, we think it is significant that Val-292 is adjacent to residues 293−298, which form a loop that undergoes a large conformational change upon the binding of coenzyme and allows the catalytic and coenzyme binding domains to move closer together (*36*). In the open and closed forms of the wild-type enzyme, Val-292 has essentially the same conformation. Ser-292 is accommodated in the open conformation without causing steric hindrance (*5*), and Thr-292 makes the same interaction with the nicotinamide ring in the closed conformation as Val-292 of the wild-type enzyme does (Figure 2). However, a new water molecule is hydrogen bonded to the hydroxyl groups of Ser-292 and Thr-292 (Figure 2), and residues in the loop are slightly shifted in both structures relative to the wild-type enzyme. After superimposing the α-carbons of the structures of the wild-type (PDB entry 8ADH) and V292S (1JU9) enzymes in the open conformation, with an rmsd of 0.36 Å, residues 292−298 superimpose with an rmsd of 0.48 Å. Likewise, after superimposing the structures of the wild-type (1N92) and V292T (1N8K) enzymes in the closed conformation, with an rmsd of 0.11 Å, residues 292−298 superimpose with an rmsd of 0.18 Å. The structural effects of the substitutions at Val-292 are subtle but apparently sufficient to perturb the energetics of the flexible loop during the conformational change so that the affinity for coenzymes is changed by 30−75-fold. For comparison, the Gly293Ala and Pro295Thr substitutions may lock the enzyme in the open form, and they decrease affinity for coenzymes 40−640-fold (*38*).

Structures of the Enzyme−NAD^+−Pyrazole Complexes. The near-atomic resolution for the structures of the V292T ADH−NAD^+−pyrazole and wild-type ADH−NAD^+−4-iodopyrazole complexes shows that the nicotinamide rings are in a boat conformation (Figures 3 and 4). The puckering is associated with the formation of a partial covalent bond between C4 of the nicotinamide ring and a nitrogen of the pyrazole. This puckered conformation may mimic the conformation of the nicotinamide ring at the transition state of the catalyzed reaction. The C3−C4 and C4−C5 bond distances (average of 1.50 Å; Table 5) reflect the change from aromatic (1.39 Å) to single bond character. Although pyrazole does not appear to be a transition-state analogue, as it does not resemble an alcohol, the geometry of the complexes (Figure 4) shows that the position of N1 of the pyrazole is close to that of O1 for a bound alcohol and N2 of pyrazole (which must be negatively charged before it reacts with the NAD^+) is close to the position expected for a hydride ion in flight.

The puckered nicotinamide ring of NAD^+ is not observed in the structure of the wild-type ADH−NAD^+−pentafluorobenzyl alcohol complex (Figure 4), and puckering has not been described before in any other structure of an enzyme complexed with NAD and a relevant substrate analogue. A twisted boat conformation has been observed for the reduced nicotinamide ring in a complex with horse liver ADH, but this seems to involve reaction of water with C6 of the nicotinamide ring (*39*). The relevance of this structure for the catalytic mechanism is not apparent because no such water is observed in other ternary complexes that resemble a Michaelis complex (PDB entries 1HLD, 1N8K, 1MG0, 1AXE, 2OHX, 1LDE, 1LDY, 1BTO, 3BTO, and 1E3I).

Quantum mechanical/molecular mechanical calculations on the oxidation of benzyl alcohol by ADH suggest that the nicotinamide ring of NAD^+ adopts a boatlike conformation in the transition state (*4*). The calculations show that the C4 and N1 atoms deviate from the plane of the other atoms in the nicotinamide ring by as much as 18° and 10°, respectively. Molecular dynamics simulations on the wild-type ADH−NADH−benzaldehyde complex show that fluctuations of the protein cause the nicotinamide ring of NADH to bend, with angles for the deviation of C4 being as large as 20° (*40*). Resonance Raman experiments that examined NADH bound to lactate dehydrogenase suggest that the nicotinamide ring of NADH attains a puckered conformation with C4 being about 15° out of the plane of the ring (*13*).

It has been argued that the nicotinamide ring does not pucker during catalysis by ADH because no secondary ^{15}N isotope effect at the N1 position of the nicotinamide ring was observed (*41*). It was expected that N1 should change bond order as the nicotinamide ring attains a boat conformation. However, computational studies on the effect of ring deformation on the aromaticity of benzene suggest that the aromatic nature is retained when the carbons are puckered out of the plane of the ring by as much as 55° (*42*). If the nicotinamide ring of NAD^+ retains its aromatic nature while puckering and there is no change in bond order, a ^{15}N secondary isotope effect at the N1 position is not expected. Nevertheless, the observation of the puckered nicotinamide ring in the ADH−NAD^+−pyrazole complexes together with the resonance Raman and computational results supports the idea that the nicotinamide ring can adopt a conformation that brings the reacting carbons of the substrates closer together and lowers the barrier for the transition state of the reaction.

Effects of the Substitutions on the Hydride Transfer Step. Substitutions of amino acid residues in the nicotinamide binding site have significant effects on the rate constant for hydride transfer from benzyl alcohol. The effects are not drastic, however, with the largest being a 16-fold decrease (Table 3). We might expect larger changes (greater than 100-fold) when a residue that interacts with a substrate is substituted. The modest effects of the substitutions suggest that no single residue in the nicotinamide binding site controls catalysis and therefore that many residues are involved in facilitating hydride transfer. The substitutions in the nicotinamide binding site could affect the rate constant for hydride transfer by decreasing the steric interactions with the nicotinamide ring, by perturbing the dynamics of the protein and nicotinamide ring, or by a combination of the two mechanisms.

The effects of the T178S, V203A, V292A, and V292S substitutions on hydride transfer are consistent with the idea that removing methyl groups from the amino acid side chains that interact with the nicotinamide ring gives the nicotinamide ring more room in which to move and to access orientations that are not productive for hydride transfer. This mobility would lead to a decrease in the rate constants for hydride transfer (*43*). The structure of the V203A ADH−NAD^+−trifluoroethanol ternary complex (*8*) shows that the increase in space behind the nicotinamide ring, due to the V203A substitution, allows the nicotinamide ring to rotate about 5−6° around the C1−N1 glycosidic bond toward the substituted residue and away from the alcohol. This results in a conformation where C4 may not be optimally oriented for hydride transfer, and the hydride donor−acceptor distance is increased, resulting in a 16-fold decrease in the rate constant for hydride transfer.

In contrast, the V292T substitution causes a 2.5-fold decrease in the rate constant for hydride transfer from benzyl alcohol (Table 3) apparently without changing the steric interactions with the nicotinamide ring (Figure 2). The decrease in the rate constant for hydride transfer could be due to the new hydrogen bond network formed between Ser-182, Thr-292, the new water molecule, and Val-290, which perturbs the dynamics at the active site (Figure 2). The relatively small decrease in the hydride transfer rate constant could mean that dynamics do not have a large role in catalysis or that the dynamics are only slightly perturbed by the V292T substitution. The isotope and temperature dependencies of the reactions catalyzed by the V292S enzyme suggest that, even with the decrease in steric interactions with the nicotinamide ring, the motions of the protein and substrates may be involved in facilitating the chemical reaction (*5*).

The lack of puckering of the nicotinamide ring in the wild-type ADH−NAD^+−pentafluorobenzyl alcohol complex, which appears to resemble the ground state of the reaction, suggests that the ring is not substantially destabilized by the ground state binding interactions. The dynamic motions of the protein, acting through the amino acid residues in the nicotinamide binding site, may assist in straining the nicotinamide ring and moving the substrates from the ground state to the transition state positions. The effects of the amino acid substitutions in the nicotinamide binding site on the rates of hydride transfer to NAD^+ (Table 3) and the movement of Thr-178 toward the nicotinamide ring (Figure 4) suggest that the interactions of the protein can assist in destabilizing the nicotinamide ring. These effects are consistent with the results from two different calculations on the reactions catalyzed by alcohol dehydrogenase, which found a correlation between the interactions of Val-203 and Thr-178 and the activation energy for the reaction (*4*) and increased fluctuations of the Val-203 and Thr-178 side chains in the transition state region of the reaction (*3*).

The V203A enzyme has diminished tunneling as compared to the wild-type enzyme (*8*), which suggests that the substitution does not allow reacting carbons to get close enough together for tunneling to occur. Since the rate constant for hydride transfer is not severely affected by the diminished tunneling (16-fold decrease), it appears that tunneling does not make a large contribution to catalysis by alcohol dehydrogenase, relative to the overall rate of acceleration caused by the enzyme. This is supported by the calculations on the reaction catalyzed by alcohol dehydrogenase, which suggest that tunneling makes a small contribution, about 2-fold, to the overall rate acceleration (*3*, *9*). However, the involvement of tunneling in the reaction is important for what it reveals about the involvement of protein and substrate dynamics in the chemical steps of the reactions catalyzed by alcohol dehydrogenase and other enzymes (*44*, *45*).

The effects of the amino acid substitutions on the enzyme kinetics suggest that the residues in the nicotinamide binding site contribute not only to the rates of hydride transfer but also to the energetics of the conformational change that occurs upon coenzyme binding. Calculations on the reactions

catalyzed by alcohol dehydrogenase suggest that the equilibrium motions of the residues in the nicotinamide binding site are coupled to the reaction coordinate for hydride transfer (*3*, *4*, *46*, *47*). However, the exact motions and their correlation with the chemical step are not known. The experimentally measured rate constants for hydride transfer should be useful information for the computational efforts that are determining the contribution of protein dynamics to catalysis by alcohol dehydrogenase.

ACKNOWLEDGMENT

We thank S. Ramaswamy for considerable assistance with the X-ray crystallography and Daniel J. Ferraro for calculating the geometry of the nicotinamide rings. We also thank The University of Iowa Macromolecular Crystallography Facility for instrumentation. Synchrotron data were collected at beamline 17-ID in the facilities of the Industrial Macromolecular Crystallography Association Collaborative Access Team (IMCA-CAT) at the Advanced Photon Source. These facilities are supported by the companies of the Industrial Macromolecular Crystallography Association through a contract with the Illinois Institute of Technology (IIT), executed through IIT's Center for Synchrotron Radiation Research and Instrumentation. Use of the Advanced Photon Source at Argonne National Laboratory was supported by the U.S. Department of Energy, Basic Energy Sciences, Office of Science, under Contract W-31-109-Eng-38. The University of Iowa DNA Facility is supported by the Diabetes and Endrocrinology Reseach Center with NIH Grant DK25295 and the Roy J. and Lucille A. Carver College of Medicine.

REFERENCES

1. Kohen, A., Cannio, R., Bartolucci, S., and Klinman, J. P. (1999) *Nature 399*, 496−499.
2. Antoniou, D., and Schwartz, S. D. (2001) *J. Phys. Chem. B 105*, 5553−5558.
3. Alhambra, C., Corchado, J., Sanchez, M. L., Garcia-Viloca, M., Gao, J., and Truhlar, D. G. (2001) *J. Phys. Chem. B 105*, 11326−11340.
4. Billeter, S. R., Webb, S. P., Agarwal, P. K., Iordanov, T., and Hammes-Schiffer, S. (2001) *J. Am. Chem. Soc. 123*, 11262−11272.
5. Rubach, J. K., Ramaswamy, S., and Plapp, B. V. (2001) *Biochemistry 40*, 12686−12694.
6. Cha, Y., Murray, C. J., and Klinman, J. P. (1989) *Science 243*, 1325−1330.
7. Bahnson, B. J., Park, D.-H., Kim, K., Plapp, B. V., and Klinman, J. P. (1993) *Biochemistry 32*, 5503−5507.
8. Bahnson, B. J., Colby, T. D., Chin, J. K., Goldstein, B. M., and Klinman, J. P. (1997) *Proc. Natl. Acad. Sci. U.S.A. 94*, 12797−12802.
9. Cui, Q., Elstner, M., and Karplus, M. (2002) *J. Phys. Chem. B 106*, 2721−2740.
10. Ramaswamy, S., Eklund, H., and Plapp, B. V. (1994) *Biochemistry 33*, 5230−5237.
11. Almarsson, O., and Bruice, T. C. (1993) *J. Am. Chem. Soc. 115*, 2125−2138.
12. Webb, S. P., Agarwal, P. K., and Hammes-Schiffer, S. (2000) *J. Phys. Chem. B 104*, 8884−8894.
13. Deng, H., Zheng, J., Sloan, D., Burgner, J., and Callender, R. (1992) *Biochemistry 31*, 5085−5092.
14. Ganzhorn, A. J., and Plapp, B. V. (1988) *J. Biol. Chem. 263*, 5446−5454.
15. Park, D.-H., and Plapp, B. V. (1991) *J. Biol. Chem. 266*, 13296−13302.
16. Theorell, H., and Yonetani, T. (1963) *Biochem. Z. 338*, 537−553.
17. Plapp, B. V. (1970) *J. Biol. Chem. 245*, 1727−1735.
18. Cleland, W. W. (1979) *Methods Enzymol. 63*, 103−138.
19. Sekhar, V. C., and Plapp, B. V. (1988) *Biochemistry 27*, 5082−5088.
20. Ramaswamy, S., Scholze, M., and Plapp, B. V. (1997) *Biochemistry 36*, 3522−3527.
21. Deng, H., Schindler, J. F., Berst, K. B., Plapp, B. V., and Callender, R. (1998) *Biochemistry 37*, 14267−14278.
22. Frieden, C. (1994) *Methods Enzymol. 240*, 311−322.
23. Andersson, P., and Pettersson, G. (1982) *Eur. J. Biochem. 122*, 559−568.
24. Theorell, H., Yonetani, T., and Sjöberg, B. (1969) *Acta Chem. Scand. 23*, 255−260.
25. Otwinowski, Z., and Minor, W. (1997) *Methods Enzymol. 276*, 307−326.
26. Navaza, J. (1994) *Acta Crystallogr. A50*, 157−163.
27. CCP4 Suite. The CCP4 Suite: Programs for Protein Crystallography (1994) *Acta Crystallogr. D50*, 760−763.
28. Jones, T. A., Zou, J. Y., Cowan, S. W., and Kjeldgaard, M. (1991) *Acta Crystallogr. A47*, 110−119.
29. Sekhar, V. C., and Plapp, B. V. (1990) *Biochemistry 29*, 4289−4295.
30. Shore, J. D., and Gutfreund, H. (1970) *Biochemistry 9*, 4655−4659.
31. Eklund, H., Samama, J.-P., and Wallén, L. (1982) *Biochemistry 21*, 4858−4866.
32. Hurley, T. D., Bosron, W. F., Stone, C. L., and Amzel, L. M. (1994) *J. Mol. Biol. 239*, 415−429.
33. Davis, G. J., Bosron, W. F., Stone, C. L., Owusu-Dekyi, K., and Hurley, T. D. (1996) *J. Biol. Chem. 271*, 17057−17061.
34. Becker, N. N., and Roberts, J. D. (1984) *Biochemistry 23*, 3336−3340.
35. Eklund, H., and Brändén, C.-I. (1979) *J. Biol. Chem. 254*, 3458−3461.
36. Eklund, H., Samama, J.-P., Wallén, L., Brändén, C.-I., Åkeson, Å., and Jones, T. A. (1981) *J. Mol. Biol. 146*, 561−587.
37. Eklund, H., Samama, J.-P., and Jones, T. A. (1984) *Biochemistry 23*, 5982−5996.
38. Ramaswamy, S., Park, D.-H., and Plapp, B. V. (1999) *Biochemistry 38*, 13951−13959.
39. Meijers, R., Morris, R. J., Adolph, H. W., Merli, A., Lamzin, V. S., and Cedergren-Zeppezauer, E. S. (2001) *J. Biol. Chem. 276*, 9316−9321.
40. Luo, J., and Bruice, T. C. (2001) *J. Am. Chem. Soc. 123*, 11952−11959.
41. Rotberg, N. S., and Cleland, W. W. (1991) *Biochemistry 30*, 4068−4071.
42. Dijkstra, F., and van Lenthe, J. H. (1999) *Int. J. Quantum Chem. 74*, 213−221.
43. Rubach, J. K., and Plapp, B. V. (2002) *Biochemistry 41*, 15770−15779.
44. Sutcliffe, M. J., and Scrutton, N. S. (2000) *Trends Biochem. Sci. 25*, 405−408.
45. Kohen, A., and Klinman, J. P. (1999) *Chem. Biol. 6*, R191−R198.
46. Villà, J., and Warshel, A. (2001) *J. Phys. Chem. B 105*, 7887−7907.
47. Caratzoulas, S., Mincer, J. S., and Schwartz, S. D. (2002) *J. Am. Chem. Soc. 124*, 3270−3276.
48. Klinman, J. P. (1972) *J. Biol. Chem. 247*, 7977−7987.
49. Weidig, C. F., Halvorson, H. R., and Shore, J. D. (1977) *Biochemistry 16*, 2961−2922.
50. Dunn, M. F., Bernhard, S. A., Anderson, D., Copeland, A., Morris, R. G., and Roque, J. P. (1979) *Biochemistry 18*, 2346−2354.
51. Fan, F., and Plapp, B. V. (1995) *Biochemistry 34*, 4709−4713.
52. Shearer, G. L., Kim, K. Y., Lee, K. M., Wang, C. K., and Plapp, B. V. (1993) *Biochemistry 32*, 11186−11194.
53. Dworschack, R. T., and Plapp, B. V. (1977) *Biochemistry 16*, 2716−2725.
54. Brunger, A. T. (1992) *Nature 355*, 472−475.
55. Guillot, B., Lecomte, C., Cousson, A., Scherf, C., and Jelsch, C. (2001) *Acta Crystallogr. D57*, 981−989.
56. Pflugrath, J. W. (1999) *Acta Crystallogr. D55*, 1718−1725.

BI0272656